

One-step syntheses of Ph₃P-substituted selenido carbonyl iron and ruthenium clusters

Part 2. Crystal structures of Fe₂(μ₂-Se₂)(CO)_{6-n}(PPh₃)_n (n = 1 or 2), Fe₃(μ₃-Se)₂(CO)₈(PPh₃) and Ru₄(μ₄-Se)₂(μ-CO)₂(CO)₈(PPh₃), and HPLC behaviour of the iron derivatives¹

Paolo Baistrocchi, Maria Careri, Daniele Cauzzi, Claudia Graiff, Maurizio Lanfranchi, Paola Manini, Giovanni Predieri*, Antonio Tiripicchio

Dipartimento di Chimica Generale ed Inorganica, Chimica Analitica, Chimica Fisica, Università di Parma, Centro di Studio per la Strutturistica Diffratometrica del CNR, Viale delle Scienze, I-43100 Parma, Italy

Received 31 May 1996

Abstract

Ph₃PSe reacts with Fe₃(CO)₁₂ giving six products (1–6) belonging to three different families of clusters: Fe₂(μ-Se₂)(CO)_{6-n}L_n (two products, 3, 5, n = 1, 2), Fe₃(μ₃-Se)₂(CO)_{9-n}L_n (three products, 1, 2, 4, n = 0–2) and Fe₃(μ₃-Se)(μ-CO)(CO)_{9-n}L_n (one product, 6, n = 2). Under the same conditions, Ru₃(CO)₁₂ affords Ru₃(μ₃-Se)₂(CO)_{9-n}(PPh₃)_n (three products 7, 8, 10, n = 1–3) and the tetra-ruthenium clusters Ru₄(μ₄-Se)₂(μ-CO)₂(CO)_{9-n}(PPh₃)_n (two products, 11, 9, n = 1, 2). The structures of the clusters 2, 3, 5 and 11 · 1/2CH₂Cl₂ have been determined by X-ray diffraction methods. The mass-spectral behaviour of iron mono- and disubstituted phosphine derivatives (2–6) is characterised by the low abundance (< 6%) of polynuclear fragments, even under NiCl conditions. Gas-phase rearrangements are considered to take place in order to explain the presence of certain peaks. The six iron derivatives are effectively separated by HPLC, the elution order depending on the degree of phosphine substitution and the kind of cluster framework.

Keywords: Iron complexes; Ruthenium complexes; Selenium complexes; Cluster complexes; Crystal structures

1. Introduction

The combination of chalcogen elements and transition metals in discrete molecular clusters is of particular interest since it often results in new coordinations and geometries and could give rise to useful models and precursors for the synthesis of new materials [1–3].

Among the methods for the synthesis of transition-metal clusters containing bridging chalcogenido ligands [4], that involving tertiary phosphine chalcogenide R₃PE (E = S, Se, Te) has been proved to be one of the most effective [5–9]. This method takes advantage of the frailty of the P=E bond, which leads to the production of phosphine-substituted chalcogenido clusters through oxidative transfer of chalcogen atoms to zero-valent metal complexes.

In the preceding paper [8], we reported on the reactions of Ph₃PSe with Fe₃(CO)₁₂ and Ru₃(CO)₁₂. In the case of iron the reaction afforded several dinuclear and trinuclear compounds, namely [Fe₂(μ-Se₂)(CO)_{6-n}L_n] (n = 1, 2), [Fe₃(μ₃-Se)₂(CO)_{9-n}L_n] (n = 0–2) and [Fe₃(μ₃-Se)(μ-CO)(CO)_{9-n}L_n] (n = 2), whereas in the case of ruthenium the same reaction was found to be quite selective giving the disubstituted trinuclear cluster [Ru₃(μ₃-Se)₂(CO)₇(PPh₃)₂] in very high yield, with minor amounts of other products, among which was the tetra-ruthenium cluster [Ru₄(μ₄-Se)₂(μ-CO)₂(CO)₇(PPh₃)₂]. The crystal structures of Fe₃(μ₃-Se)(μ-CO)(CO)₇(PPh₃)₂, M₃(μ₃-Se)₂(CO)₇(PPh₃)₂ (M = Fe or Ru) and Ru₄(μ₄-Se)₂(μ-CO)₂(CO)₇(PPh₃)₂ were determined by X-ray diffraction methods.

Furthermore, we found [9] that the diphosphine diselenide CH₂(Ph₂PSe)₂ and [Ru₃(CO)₁₂] react in toluene to give (besides [Ru₃(μ₃-Se)₂(CO)₇(dppm)] and [Ru₄(μ₄-

* Corresponding author.

¹ For Part 1 see Ref. [8].

Se)₂(CO)₉(dppm)] [Ru₄(μ₃-Se)₄(CO)₁₀(dppm)] (dppm = Ph₂PCH₂PPh₂), which is the first reported 72-electron Ru–Se cubane-like cage complex.

With the present paper we wish to complete the description of the selenido clusters derived from Ph₃PSe by discussing their mass-spectral data and the high-performance liquid chromatographic (HPLC) behaviour of the iron derivatives. Furthermore, the crystal structures of the other four clusters will be described.

2. Experimental

Details on materials and standard analytical equipment were reported in the preceding paper [8]. ⁷⁷Se NMR spectra (CDCl₃ solutions) were recorded on a Bruker CXP 200 instrument operating at 38.2 MHz, using Ph₃Se₂ in CDCl₃ (+ 461 ppm relative to Me₂Se) as external reference [10].

2.1. Reactions of Ph₃PSe with M₃(CO)₁₂

Under the conditions described in Ref. [8], the reaction between Ph₃PSe and Fe₃(CO)₁₂ (2:1) gave the following products, in order of TLC elution (yields based on iron carbonyl): Fe₃(μ₃-Se)₂(CO)₉ (**1**, 27.5%); Fe₃(μ₃-Se)₂(CO)₈(PPh₃) (**2**, 36%); Fe₂(μ-Se)₂(CO)₅(PPh₃) (**3**, 6.5%); Fe₃(μ₃-Se)₂(CO)₇(PPh₃)₂ (**4**, 9%); Fe₂(μ-Se)₂(CO)₄(PPh₃)₂ (**5**, 4.5%); Fe₃(μ₃-Se)(μ-CO)(CO)₇(PPh₃)₂ (**6**, 3%). The same 2:1 reaction with Ru₃(CO)₁₂ afforded the following products, in order of elution: Ru₃(μ₃-Se)₂(CO)₈(PPh₃) (**7**, 2%); Ru₃(μ₃-Se)₂(CO)₇(PPh₃)₂ (**8**, 91.5%); Ru₄(μ₄-Se)₂(μ-CO)₂(CO)₇(PPh₃)₂ (**9**, 2.5%); Ru₃(μ₃-Se)₂(CO)₆(PPh₃)₃ (**10**, 2.5%).

With a 1:1 molar ratio the reaction lacked in selectivity. Nevertheless it was possible to separate and characterise the main product Ru₄(μ₄-Se)₂(μ-CO)₂(CO)₈(PPh₃) (**11**, 21%, reddish-brown). Suitable crystals for X-ray analysis were obtained as described in Ref. [8]. Compound **11**: IR (KBr) ν(CO): 2068s, 2033sh, 2028vs, 2014sh, 2003m,

1992m, 1970m, 1868m, 1837s; ³¹P NMR (CHCl₃-d₁, H₃PO₄): δ = 54.3 ppm.

Characterisation data for compounds **1–10** (electronic absorption maxima, ν(CO) stretching bands and ³¹P NMR peaks) have been already published [8]. Compound **2** exhibits the ⁷⁷Se resonance at δ = 243 ppm, while compound **3** exhibits a doublet centred at δ = 581 ppm (*J*(⁷⁷Se–³¹P) = 11 Hz).

2.2. Mass spectrometry

A Hewlett-Packard model 5989A system provided with a Hewlett-Packard model 59980A particle beam interface was used for mass spectra acquisition of all compounds except **8** and **10**. The flow-injection mode was used for sample introduction; for this purpose, dichloromethane solutions of the substances were injected using a Hewlett-Packard model 1090 HPLC pump; the flow rate of the eluent (CH₂Cl₂/hexane 30:70) was 0.4 cm³ min⁻¹. Helium pressure for particle beam interface was 40 psi; temperature of the interface was 45°C.

The mass spectrometer was equipped with a dual electron impact (EI)/chemical ionisation (CI) ion source, a hyperbolic quadrupole mass analyser, a continuous dinode electron multiplier detector and a differentially pumped vacuum system with diffusion pumps. The HP MS 59940A ChemStation (HP-UX series) was used as analytical workstation. The CI source temperature was held at 260°C, which was the optimum value; methane was used as the reagent gas; the ionisation energy was 230 eV and the voltage applied to the electron multiplier was 2100 V. Both positive and negative ions were monitored. The quadrupole temperature was maintained at 100°C; for scan acquisition the system was scanned from 150 to 900 a.m.u.

For compounds **8** and **10** a Finnigan MAT SSG710 spectrometer equipped with an EI/CI source, a direct inlet system and a quadrupole mass analyser was used. The CI source was utilised with methane as the reagent gas (T source, 220°C; methane ionisation energy, 70 eV). The quadrupole temper-

Table 1

Main fragments and relative abundances observed in the negative-ion chemical-ionization (NICI) mass spectra of the iron clusters **1–6**

<i>m/z</i>	Ion	1	2	3	4	5	6
168	[Fe(CO) ₄] ⁻	100	100	100	100	67	14
262	[PPh ₃] ⁻		1	16	<1	49	3
297	[Fe ₂ Se ₂ (CO)] ⁻	1		5		3	
326	[Fe ₃ Se] ⁻	13	1		2		
326	[Fe ₂ Se ₂ (CO) ₂] ⁻			52		8	11
346	[Fe(PPh ₃)(CO)] ⁻		1		1	12	7
374	[Fe(PPh ₃) ₂ (CO) ₂] ⁻				2	9	5
402	[Fe(PPh ₃) ₂ (CO)] ⁻		9	7	7	100	100
437	[Fe ₂ Se ₂ (CO) ₄] ⁻	4			1		1
465	[Fe ₃ Se ₂ (CO) ₃] ⁻	6			2		2
493	[Fe ₃ Se ₂ (CO) ₆] ⁻	20	2		3		2
521	[Fe ₃ Se ₂ (CO) ₇] ⁻	74	4		6		4
549	[Fe ₂ Se ₂ (CO) ₈] ⁻	<1					

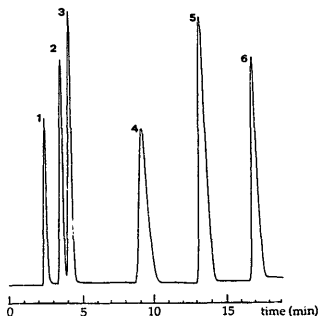


Fig. 1. HPLC separation of the iron clusters 1–6 under the conditions described in Section 2.

ature was maintained at 140°C; the system was scanned from 550 to 1500 a.m.u. and both positive (PICI) and negative ion (NICI) spectra were recorded. Table 1 and Fig. 3 report the most significant ionic fragments, obtained in NICI mode, for the iron clusters 1–6 and the ruthenium cluster 8, respectively.

Table 2
Summary of crystallographic data for complexes 2, 3, 5 and 11 · 0.5CH₂Cl₂

	2	3	5	11 · 0.5CH ₂ Cl ₂
Formula	C ₂₀ H ₁₂ Fe ₂ O ₈ PSe ₂	C ₂₃ H ₁₃ Fe ₂ O ₈ PSe ₂	C ₄₀ H ₂₀ Fe ₂ O ₈ P ₂ Se ₂	C ₂₈ H ₁₅ O ₁₀ PRu ₄ Se ₂ · 0.5CH ₂ Cl ₂
Molecular weight	811.83	671.96	906.24	1147.06
Crystal system	triclinic	triclinic	monoclinic	monoclinic
Space group	P1	P1	C2/c	P2 ₁ /n
Radiation (Mo Kα λ = 0.71073 Å)	graphite monochromated	Nb-filtered	Nb-filtered	graphite monochromated
a (Å)	9.947(2)	8.092(4)	19.477(8)	13.652(3)
b (Å)	16.922(4)	16.366(8)	10.212(5)	21.675(5)
c (Å)	8.941(2)	9.603(5)	19.603(7)	24.315(5)
α (°)	96.85(2)	91.62(2)		
β (°)	93.82(2)	98.68(2)	101.70(2)	105.03(2)
γ (°)	105.06(2)	103.17(2)		
V (Å ³)	1435.4(6)	1222(1)	3818(3)	6949(3)
Z	2	2	4	8
D _{calc} (g cm ⁻³)	1.878	1.827	1.577	2.193
F(000)	792	656	1808	4344
Crystal size (nm)	0.15 × 0.19 × 0.21	0.16 × 0.18 × 0.22	0.11 × 0.15 × 0.21	0.10 × 0.25 × 0.35
μ (Mo Kα) (cm ⁻¹)	41.34	42.64	27.90	39.75
Diffractometer	Philips PW 1100	Siemens AED	Siemens AED	Philips PW 1100
Scan type	θ/2θ	θ/2θ	θ/2θ	θ/2θ
Scan speed (° min ⁻¹)	3–10	3–12	3–12	3–10
θ Range (°)	3–30	3–25	3–27	3–24
Standard reflections	one measured after 100	one measured after 100	one measured after 100	one measured after 100
Reflections measured	± h, ± k, l	± h, ± k, l	± h, k, l	± h, k, l
Unique total data	8368	4307	4230	10879
Unique observed data	4432 (I > 2σ(I))	2336 (I > 2σ(I))	2192 (I > 2σ(I))	3733 (I > 2σ(I))
R ^a	0.0417	0.0691	0.0441	0.0569
R _w ^b	0.0500	0.0689	0.0461	0.0708

^a R = Σ||F_o| - |F_c|| / Σ|F_o|.

^b R_w = {Σw(|F_o| - |F_c||)² / Σw(F_o)²}^{1/2}.

2.3. High-performance liquid chromatography

For the chromatographic separations a Perkin-Elmer 250 chromatograph, equipped with a Rheodyne 7125 injection valve and a Perkin-Elmer LC-75 variable-wavelength UV-Vis detector, was used. Dichloromethane solutions of the compounds (20 μl) were injected into a stainless steel column (25 cm × 0.4 cm i.d.) filled with 5 μm LiChrosorb Si 60 (Merck), monitoring the eluates at 288 nm. The separation of the six iron derivatives 1–6, shown in Fig. 1, required two elution steps: a linear gradient, starting from a CH₂Cl₂/hexane 18:82 mixture to a 30:70 mixture in 10 min, was followed by an isocratic elution, with the last eluent composition, for 7 min. The flow rate was 1 cm³ min⁻¹.

2.4. X-ray data collection, structure solution and refinement

The crystallographic data for compounds 2, 3, 5 and 11 · 1/2CH₂Cl₂ are summarized in Table 2. Accurate unit cell parameters were obtained by using the setting angles of 30 high-angle reflections. One standard reflection was monitored every 100 measurements; no significant decay was noticed over the time of data collection. Intensities were corrected for Lorentz and polarisation effects. A correction for absorp-

tion was applied for **2**, **3** and **11** · 1/2CH₂Cl₂ (maximum and minimum values for the transmission coefficients were 1.000 and 0.6467, 1.000 and 0.6777, 1.000 and 0.4500, respectively) [11].

All four structures were solved by Patterson methods of SHELXS-86 [12] and refined by full-matrix least-squares, using the SHELX-76 program [13], first with isotropic thermal parameters and then with anisotropic thermal parameters for all non-hydrogen atoms for **3** and **5**, only for Se, Fe, P atoms and CO groups for **2**, and for Se, Ru and P atoms for **11** · 1/2CH₂Cl₂. The phenyl rings of the PPh₃ group of **2** were found disordered and distributed in two positions with equal occupancy factor; for this reason the positions for the hydrogen atoms were not calculated. Disordered dichloromethane molecules of solvation were found in the crystals of **11** · 1/2CH₂Cl₂. The hydrogen atoms of **3**, **5** and **11** · 1/2CH₂Cl₂ were placed at their geometrically calculated positions (C–H = 0.96 Å) and refined 'riding' on the corresponding carbon atoms, except those of the solvent for **11** · 1/2CH₂Cl₂. The final cycles of refinement were carried out on the basis of 271 variables for **2**, 301 for **3**, 227 for **5** and 449 for **11** · 1/2CH₂Cl₂. The biggest remaining peak (close to one heavy atom) in the final difference map was equivalent to about 0.86 e Å⁻³ for **2**, 0.80 for **3**, 0.56 for **5** and 2.33 for **11** · 1/2CH₂Cl₂. A weighting scheme $w = K[\sigma^2(F_o) + gF_o^2]^{-1}$ was used in the last cycles of refinement with $K = 2.051$ and $g = 0.0003$ (**2**), $K = 6.340$ and $g = 0.0002$ (**3**), $K = 1.995$ and $g = 0.0004$ (**5**), $K = 7.338$ and $g = 0.0002$ (**11** · 1/2CH₂Cl₂) at convergence. Atomic scattering factors and anomalous scattering coefficients were taken from Ref. [14]. All calculations were carried out on the GOULD POWERNODE 6040 and ENCORE 91 computers of the 'Centro di Studio per la Strutturistica Diffattometrica' del C.N.R., Parma. See also Section 4.

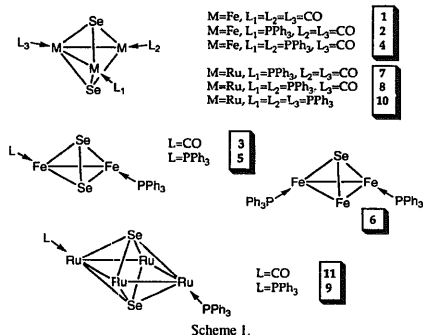
3. Results and discussion

The reactions of Ph₃PSe with Fe₃(CO)₁₂ and Ru₃(CO)₁₂ produce a variety of Ph₃P-substituted selenido carbonyl clusters, whose structural frameworks are represented in Scheme 1 (carbonyl ligands omitted).

It is reasonable to think that compounds **4** and **8**, M₃(μ₃-Se)₂(CO)₇(PPh₃)₂ (M = Fe or Ru), are the primary products of the oxidative attack of two molecules of Ph₃PSe to the metal carbonyl triangles, whereas the other compounds derive from secondary reactions, which probably take place under the adopted reaction conditions [8]. In the 1:1 reaction involving ruthenium, the overall yield in selenido clusters is significantly lower than in the 2:1 experiment and the main products are the mono-substituted derivatives **7** and **11**.

3.1. Mass spectra

The mass spectra of the iron compounds **1–6** were obtained both in positive-ion (PI) and negative-ion (NI) chemical



ionization (CI) mode. Under PICI conditions, the mass spectra of the polynuclear organoiron compounds are characterized by low-mass fragments, due to the PPh₃ ligand ([PPh₂]⁺ and [HPPH₃]⁺, *m/z* = 185, 263, respectively) and to mononuclear iron fragments, such as [Fe(CO)_{*n*}(PPh₃)_{*n*}]⁺ (*n* = 1–4).

The results obtained under NICI conditions are summarised in Table 1. The most abundant ions (100%) are attributable to the tetracarbonyl mononuclear fragments [Fe(CO)₄]⁻ (compounds **1–4**) and [Fe(CO)₃(PPh₃)]⁻ (compounds **5, 6**) at *m/z* = 168 and 402, respectively. Molecular ions are not detected in any cases. This behaviour emphasises the low stability of the iron clusters, particularly for the mono- and diphosphine derivatives, for which polynuclear metal fragments are present with low abundance (1–6%).

A gas-phase rearrangement involving the cluster **6** core is necessary to explain the origin of some peaks containing two selenium atoms, particularly the abundant family of peaks centred at *m/z* = 326 (11%). It may be confidently attributed to the [Fe₂Se₂(CO)₂]⁻ ion by comparison between the experimental isotopic pattern with the corresponding calculated pattern shown in Fig. 2.

Concerning the ruthenium complexes **8** and **10**, the PICI mass spectra show the molecular ions together with several groups of peaks at 28-μ intervals, arising from the progressive loss of the carbonyl ligands (e.g. [Ru₃Se₂(CO)₇(PPh₃)₂]⁺, *m/z* 1153, 100% for **8** and 73% for **10**). The considerable abundance of the molecular ions, particularly for compound **8** (49%), is related to the higher stability of the ruthenium clusters compared to the iron homologues.

In the NICI spectra of **8** and **10** the highest-mass signal is attributable to [M–CO]⁻, whereas the most intense signal, detected at *m/z* = 920 for both compounds, is due to the fragment [Ru₃Se₂(CO)₇(PPh₃)]⁻. For **10** the formation of this apparently stable fragment requires gas-phase rearrangements in the ligand sphere. The fragmentation paths of compound **8** in NICI mode are illustrated in Fig. 3.

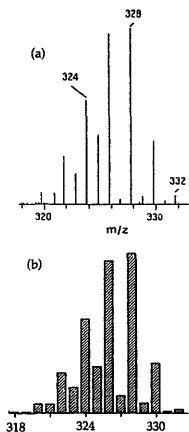


Fig. 2. Found (a) and calculated (b) isotopic patterns for the fragment $[\text{Fe}_2\text{Se}_2(\text{CO})_2]^+$.

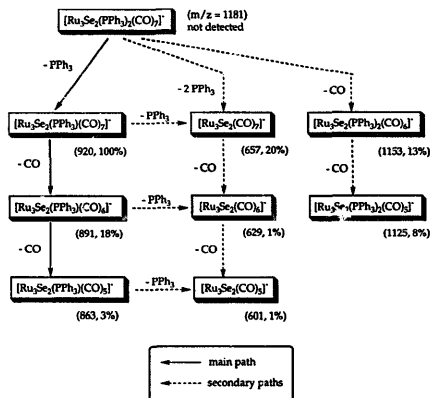


Fig. 3. Fragmentation patterns of compound **8** in NICI mode.

3.2. HPLC behaviour

The use of HPLC for preparative and analytical separations of mono- and polynuclear organometallic compounds has rapidly increased in recent years, owing to its superior efficiency compared with traditional column and thin layer chromatography [15]. Recent progresses in this field include the separation of enantiomeric 'chiral-at-metal' cyclopentadienyl complexes [16] and the successful application of the combined technique HPLC-MS for the simultaneous separation and identification of carbonyl clusters [17].

The chromatogram shown in Fig. 1 suggests that the chromatographic behaviour, under normal-phase conditions, of

the selenido-carbonyl iron derivatives depends on two main factors: (i) the degree of phosphine substitution; (ii) the cluster framework.

Regarding the first one, the substitution of CO with PPh_3 causes longer retention times, as already observed [18], owing to the presence of the slightly polar phenyl rings, which, in addition, increase the molecular surface area and the steric hindrance of the substituted clusters. This results in the excellent separations inside the two groups of the isostructural clusters **1**, **2**, **4** and **3**, **5** containing an increasing number of PPh_3 ligands. In fact, for the disubstituted compounds **4**, **5** and **6** the interactions with the silica surface appear relatively so strong that the polarity of the mobile phase has to be increased during the elution, in order to obtain the rapid, simultaneous separation of all the clusters **1–6**.

The second effect is responsible for the satisfactory separation inside the monosubstituted **2**, **3** and the disubstituted **4**, **5**, **6** groups of compounds, according to the different structural frameworks. The order of elution **4**, **5**, **6** suggests the order of polarity inside this group, cluster **6**, with a single capping selenium atom, being the most polar one.

3.3. Description of the crystal structures

The molecular structures of $\text{Fe}_2(\mu\text{-Se}_2)(\text{CO})_5(\text{PPh}_3)$ (**3**), $\text{Fe}_2(\mu\text{-Se}_2)(\text{CO})_4(\text{PPh}_3)_2$ (**5**), $\text{Fe}_2(\mu\text{-Se})_2(\text{CO})_8(\text{PPh}_3)$ (**2**) and $\text{Ru}_4(\mu_4\text{-Se})_2(\mu\text{-CO})_2(\text{CO})_8(\text{PPh}_3)$ (**11**) are shown in Figs. 4–7, respectively, together with the atomic labelling systems. The most important bond distances and angles are given in Tables 3–6, respectively.

Complex **3** (Fig. 4) exhibits an Fe_2Se_2 tetrahedral core, in which the Fe–Fe and Se–Se bond distances are 2.602(2) and 2.297(2) Å, respectively, whereas the values of the Fe–Se interactions range between 2.365(2) and 2.378(3) Å. Considering the $\mu\text{-Se}_2$ group a six-electron donor ligand, the molecule is a normal 34-electron species, with each iron atom piumped in a rather distorted octahedral environment determined by the other iron atom, the side-on bonded Se_2 group and three appropriate two-electron ligands. The phosphine ligand linked to Fe(1) replaces the carbonyl ligand in *trans*

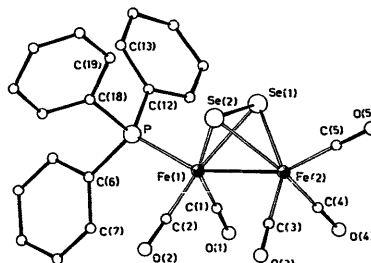


Fig. 4. Perspective view of the structure of the complex $\text{Fe}_2(\mu\text{-Se}_2)(\text{CO})_5(\text{PPh}_3)$ (**3**) with the atomic labelling scheme.

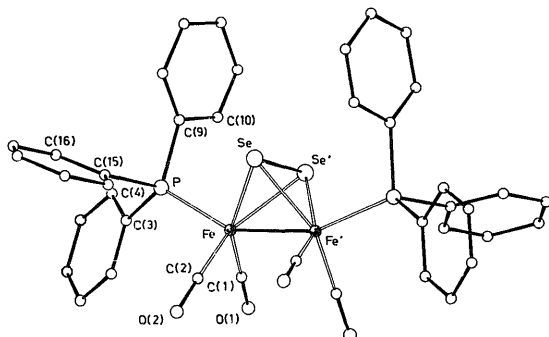


Fig. 5. Perspective view of the structure of the complex $\text{Fe}_2(\mu\text{-Se}_2)(\text{CO})_4(\text{PPh}_3)_2$ (5) with the atomic labelling scheme.

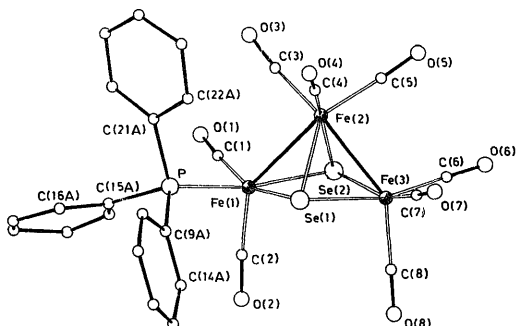


Fig. 6. Perspective view of the structure of the complex $\text{Fe}_3(\mu_3\text{-Se})_2(\text{CO})_8(\text{PPh}_3)_2$ (2) with the atomic labelling scheme.

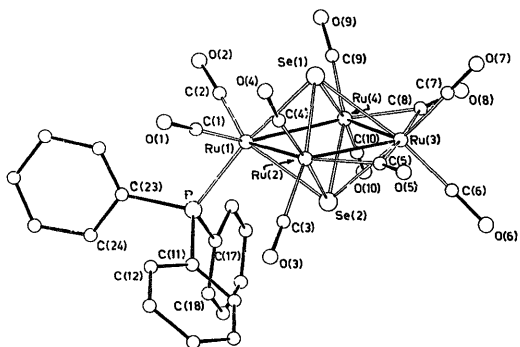


Fig. 7. Perspective view of the structure of the complex $\text{Ru}_4(\mu_3\text{-Se})_2(\mu\text{-CO})_2(\text{CO})_8(\text{PPh}_3)_4$ (11) with the atomic labelling scheme.

Table 3
Selected bond distances (Å) and angles (°) for complex 3

Se(1)–Se(2)	2.297(2)	Fe(1)–Fe(2)	2.602(2)
Se(1)–Fe(1)	2.365(2)	Se(2)–Fe(1)	2.374(3)
Se(1)–Fe(2)	2.368(2)	Se(2)–Fe(2)	2.378(3)
Fe(1)–P(1)	2.241(3)		
Fe(1)–Se(1)–Fe(2)	66.7(1)	Fe(1)–Se(2)–Fe(2)	66.4(1)
Se(2)–Se(1)–Fe(2)	61.3(1)	Se(2)–Se(1)–Fe(1)	61.2(1)
Se(1)–Se(2)–Fe(2)	60.8(1)	Se(1)–Se(2)–Fe(1)	60.8(1)
Se(1)–Fe(1)–Se(2)	58.0(1)	Fe(2)–Fe(1)–P(1)	155.1(1)
Se(2)–Fe(1)–Fe(2)	56.9(1)	Se(1)–Fe(2)–Se(2)	57.9(1)
Se(2)–Fe(1)–P(1)	104.4(1)	Se(2)–Fe(2)–Fe(1)	56.7(1)
Se(1)–Fe(1)–Fe(2)	56.7(1)	Se(1)–Fe(2)–Fe(1)	56.6(1)
Se(1)–Fe(1)–P(1)	100.3(1)		

Table 4
Selected bond distances (Å) and angles (°) for complex 5

Se–Se'	2.296(1)	Se–Fe	2.370(1)
Se–Fe'	2.389(1)	Fe–Fe'	2.595(1)
Fe–P	2.231(2)		
Fe–Se–Fe'	66.1(1)	Se–Se'–Fe'	61.6(1)
Se–Fe–Se'	57.7(1)	Se'–Se–Fe'	60.8(1)
Se'–Fe–C(2)	105.6(2)	Se'–Fe–C(1)	155.2(2)
Se'–Fe–P	95.3(1)	Se–Fe–P	105.4(1)
P–Fe–C(2)	101.3(2)	P–Fe–C(1)	98.1(2)
Se–Fe–C(2)	149.4(2)	Se–Fe–C(1)	98.6(2)
Fe'–Fe–C(2)	92.2(2)	Fe'–Fe–C(1)	106.4(2)
Se'–Fe'–Fe	57.3(1)	Fe'–Fe–P	151.5(1)
C(1)–Fe–C(2)	92.1(3)		

' = -x, y, 1/2 - z.

Table 5
Selected bond distances (Å) and angles (°) for complex 2

Se(1)–Fe(1)	2.343(1)	Se(2)–Fe(1)	2.369(1)
Se(1)–Fe(2)	2.376(1)	Se(2)–Fe(2)	2.387(1)
Se(1)–Fe(3)	2.370(1)	Se(2)–Fe(3)	2.372(1)
Fe(1)–Fe(2)	2.725(1)	Fe(2)–Fe(3)	2.611(1)
Fe(1)–P	2.272(1)		
Fe(2)–Se(1)–Fe(3)	66.8(1)	Fe(2)–Se(2)–Fe(3)	66.6(1)
Fe(1)–Se(1)–Fe(3)	98.0(1)	Fe(1)–Se(2)–Fe(3)	97.2(1)
Fe(1)–Se(1)–Fe(2)	70.6(1)	Fe(1)–Se(2)–Fe(2)	69.9(1)
Se(1)–Fe(1)–Se(2)	82.1(1)	Se(2)–Fe(2)–Fe(1)	54.7(1)
Se(2)–Fe(1)–P	167.6(1)	Se(1)–Fe(2)–Fe(1)	54.2(1)
Se(2)–Fe(1)–Fe(2)	55.3(1)	Se(1)–Fe(2)–Se(2)	81.0(1)
Se(1)–Fe(1)–P	93.0(1)	Fe(1)–Fe(2)–Fe(3)	83.5(1)
Se(1)–Fe(1)–Fe(2)	55.3(1)	Se(2)–Fe(2)–Fe(3)	56.4(1)
Fe(2)–Fe(1)–P	112.6(1)	Se(1)–Fe(2)–Fe(3)	56.5(1)
Se(2)–Fe(3)–Fe(2)	57.0(1)	Se(1)–Fe(3)–Se(2)	81.4(1)
Se(1)–Fe(3)–Fe(2)	56.7(1)		

position with respect to the other iron atom. As expected the whole structure is very similar to that of the unsubstituted complex $\text{Fe}_2\text{Se}_2(\text{CO})_6$ [19], the only significant difference being the value of the Fe–Fe distance, which in the hexacarbonyl cluster is slightly shorter, 2.575(1) Å.

The structure of the disubstituted complex 5 (Fig. 5) is strictly comparable with that of 3, from which it derives by substitution of the other carbonyl collinear with the Fe–Fe

Table 6
Selected bond distances (Å) and angles (°) for complex 11-0.5CH₂Cl₂

Molecule 1		Molecule 2	
Ru(11)–Ru(21)	2.840(3)	Ru(12)–Ru(22)	2.829(3)
Ru(11)–Ru(41)	2.875(3)	Ru(12)–Ru(42)	2.879(3)
Ru(11)–Se(11)	2.594(3)	Ru(12)–Se(12)	2.588(3)
Ru(11)–Se(21)	2.564(3)	Ru(12)–Se(22)	2.562(4)
Ru(11)–P(11)	2.329(7)	Ru(12)–P(12)	2.338(7)
Ru(21)–Ru(31)	2.784(3)	Ru(22)–Ru(32)	2.778(3)
Ru(21)–Se(11)	2.570(3)	Ru(22)–Se(12)	2.560(4)
Ru(21)–Se(21)	2.595(3)	Ru(22)–Se(22)	2.592(4)
Ru(31)–Ru(41)	2.777(3)	Ru(32)–Ru(42)	2.780(3)
Ru(31)–Se(11)	2.643(3)	Ru(32)–Se(12)	2.634(4)
Ru(31)–Se(21)	2.615(3)	Ru(32)–Se(22)	2.598(3)
Ru(41)–Se(11)	2.554(4)	Ru(42)–Se(12)	2.560(4)
Ru(41)–Se(21)	2.572(3)	Ru(42)–Se(22)	2.579(3)
Se(21)–Ru(11)–P(11)	91.7(2)	Se(22)–Ru(12)–P(12)	91.5(2)
Se(11)–Ru(11)–P(11)	170.8(2)	Se(12)–Ru(12)–P(12)	171.0(2)
Se(11)–Ru(11)–Se(21)	79.6(1)	Se(12)–Ru(12)–Se(22)	79.5(1)
Ru(41)–Ru(11)–P(11)	121.7(2)	Ru(42)–Ru(12)–P(12)	119.2(2)
Ru(41)–Ru(11)–Se(21)	56.1(1)	Ru(42)–Ru(12)–Se(22)	56.2(1)
Ru(41)–Ru(11)–Se(11)	55.4(1)	Ru(42)–Ru(12)–Se(12)	55.5(1)
Ru(21)–Ru(11)–P(11)	116.4(2)	Ru(22)–Ru(12)–P(12)	118.6(2)
Ru(21)–Ru(11)–Se(21)	57.1(1)	Ru(22)–Ru(12)–Se(22)	57.2(1)
Ru(21)–Ru(11)–Se(11)	56.3(1)	Ru(22)–Ru(12)–Se(12)	56.2(1)
Ru(21)–Ru(11)–Ru(41)	87.3(1)	Ru(22)–Ru(12)–Ru(42)	87.6(1)
Ru(11)–Ru(21)–Se(21)	56.1(1)	Ru(12)–Ru(22)–Se(22)	56.2(1)
Ku(11)–Ru(21)–Se(11)	57.0(1)	Ru(12)–Ru(22)–Se(12)	57.1(1)
Ru(11)–Ru(21)–Ru(31)	91.5(1)	Ru(12)–Ru(22)–Ru(32)	91.4(1)
Se(11)–Ru(21)–Se(21)	79.4(1)	Se(12)–Ru(22)–Se(22)	79.4(1)
Ru(31)–Ru(21)–Se(21)	58.0(1)	Ru(32)–Ru(22)–Se(22)	57.7(1)
Ru(31)–Ru(21)–Se(11)	59.0(1)	Ru(32)–Ru(22)–Se(12)	59.0(1)
Ru(21)–Ru(31)–Se(21)	57.4(1)	Ru(22)–Ru(32)–Se(22)	57.5(1)
Ru(21)–Ru(31)–Se(11)	56.5(1)	Ru(22)–Ru(32)–Se(12)	56.4(1)
Ru(21)–Ru(31)–Ru(41)	90.3(1)	Ru(22)–Ru(32)–Ru(42)	90.6(1)
Se(11)–Ru(31)–Se(21)	77.8(1)	Se(12)–Ru(32)–Se(22)	78.0(1)
Ru(41)–Ru(31)–Se(21)	56.9(1)	Ru(42)–Ru(32)–Se(22)	57.2(1)
Ru(41)–Ru(31)–Se(11)	56.2(1)	Ru(42)–Ru(32)–Se(12)	56.4(1)
Ru(11)–Ru(41)–Ru(31)	90.9(1)	Ru(12)–Ru(42)–Ru(32)	90.3(1)
Ru(31)–Ru(41)–Se(21)	58.4(1)	Ru(32)–Ru(42)–Se(22)	57.8(1)
Ru(31)–Ru(41)–Se(11)	59.3(1)	Ru(32)–Ru(42)–Se(12)	58.9(1)
Ru(11)–Ru(41)–Se(21)	55.8(1)	Ru(12)–Ru(42)–Se(22)	55.7(1)
Ru(11)–Ru(41)–Se(11)	56.7(1)	Ru(12)–Ru(42)–Se(12)	56.5(1)
Se(11)–Ru(41)–Se(21)	80.2(1)	Se(12)–Ru(42)–Se(22)	79.7(1)
Ru(31)–Se(11)–Ru(41)	64.6(1)	Ru(32)–Se(12)–Ru(42)	64.7(1)
Ru(21)–Se(11)–Ru(41)	100.6(1)	Ru(22)–Se(12)–Ru(32)	64.6(1)
Ru(21)–Se(11)–Ru(31)	64.5(1)	Ru(22)–Se(12)–Ru(32)	64.6(1)
Ru(11)–Se(11)–Ru(41)	67.9(1)	Ru(12)–Se(12)–Ru(42)	68.0(1)
Ru(11)–Se(11)–Ru(31)	100.5(1)	Ru(12)–Se(12)–Ru(32)	100.4(1)
Ru(11)–Se(11)–Ru(21)	66.7(1)	Ru(12)–Se(12)–Ru(22)	66.7(1)
Ru(31)–Se(21)–Ru(41)	64.7(1)	Ru(32)–Se(22)–Ru(42)	65.0(1)
Ru(21)–Se(21)–Ru(41)	99.5(1)	Ru(22)–Se(22)–Ru(42)	99.7(1)
Ru(21)–Se(21)–Ru(31)	64.6(1)	Ru(22)–Se(22)–Ru(32)	64.7(1)
Ru(11)–Se(21)–Ru(41)	68.1(1)	Ru(12)–Se(22)–Ru(42)	68.1(1)
Ru(11)–Se(21)–Ru(31)	102.1(1)	Ru(12)–Se(22)–Ru(32)	102.1(1)
Ru(11)–Se(21)–Ru(21)	66.8(1)	Ru(12)–Se(22)–Ru(22)	66.6(1)

vector. The molecule has a crystallographic symmetry C_2 with the binary axis passing through the midpoints of the two Fe–Fe and Se–Se bonds. The substitution of the second carbonyl with PPh₃ does not cause significant structural alterations to the cluster framework, all the important distances being practically unchanged with respect to 3.

The monosubstituted cluster 2 has a Se-bicapped open triangular 50-electron iron framework, with the phosphine

ligand occupying a *trans* position to an Fe–Se bond. The geometry of the Fe_3Se_2 core can be described as a square pyramid with two Fe and two Se atoms alternating in the basal plane and the third Fe atom at the vertex. In the crystals the PPh₃ ligand is disordered in such a way that phenyl rings are disposed in two different positions (A and B). Fig. 6 shows the phenyls in A positions. The two Fe(1)–Fe(2) and Fe(2)–Fe(3) separations, 2.724(2) and 2.614(2) Å, respectively, are rather different, that involving the iron atom Fe(1) bound to the phosphine being longer. It is interesting to note that these bond distances in the unsubstituted cluster $\text{Fe}_3\text{Se}_2(\text{CO})_9$ (1), 2.64(2) and 2.66(2) Å [20], are intermediate between those observed in **2**. On the contrary, the other interatomic contacts, such as the Fe–Se bond distances (which span between 2.345(2) and 2.392(2) in **2** and between 2.34(2) and 2.37(2) Å in **1**) and the Fe(1)⋯Fe(3) non-bonding separation (3.556(2) in **2** and 3.51(2) Å in **1**) are well comparable.

The crystal structure of the complex $\text{Ru}_4(\mu_4\text{-Se})_2(\mu\text{-CO})_2(\text{CO})_8(\text{PPh}_3)$ (**11**) is characterised by the presence of two independent, even if very similar, molecules in the unit cell; Fig. 7 shows the structure of molecule **1**.

Complex **11** exhibits a distorted *closo*-octahedral Ru_4Se_2 core with seven skeletal electron pairs. Two carbonyls asymmetrically bridge two adjacent Ru–Ru edges, which are the shortest of the four Ru–Ru bond distances (Ru(2)–Ru(3) = 2.784(3) [2.778(3)] and Ru(3)–Ru(4) = 2.777(3) [2.780(3)] Å, heretofore the values in brackets refer to the second molecule). All the ruthenium atoms are also bonded to two terminal carbonyls. The atom Ru(3) bound to the bridging ligands displays the longest bond distances with both Se atoms (Ru(3)–Se(1) = 2.643(3) [2.634(4)] and Ru(3)–Se(2) = 2.615(3) [2.598(3)] Å). A phosphine ligand is bonded to the Ru(1) atom, *trans* to the Ru(1)–Se(1) bond.

The structure of complex **11** is comparable to those of unsubstituted [21] and disubstituted **9** [8] analogues. In complex **9**, one of the two phosphine ligands occupies the same position *trans* to the Ru(1)–Se(1) bond and the substitution of the second phosphine on Ru(3) does not cause appreciable changes in the bond distances with both Se, Ru(2) and Ru(3) atoms.

4. Supplementary material

The final coordinates for the non-hydrogen atoms with the equivalent isotropic displacement parameters, U_{eq} , those for the hydrogen atoms with the isotropic thermal parameters,

anisotropic thermal parameters, and observed and calculated structure factors are available from the Cambridge Crystallographic Data Center or from the authors on request.

Acknowledgements

Financial support from M.U.R.S.T. (Rome) is gratefully acknowledged. The facilities of the Centro Interdipartimentale di Misure (Università di Parma) were used to record the NMR spectra and the mass spectra of the ruthenium derivatives.

References

- [1] G. Longoni and M.C. Iapalucci, in G. Schmid (ed.), *Clusters and Colloids*, VCH, Weinheim, 1994, p. 132; D. Fenske, p. 212.
- [2] M.L. Steigerwald, *Polyhedron*, **13** (1994) 1245.
- [3] P. Mathur, Md.M. Hossain, P.B. Hitchcock and J.F. Nixon, *Organometallics*, **14** (1995) 3101.
- [4] L.C. Roof and J.W. Kolis, *Chem. Rev.*, **93** (1993) 1037.
- [5] G. Hogarth, N.J. Taylor, A.J. Carty and A. Meyer, *J. Chem. Soc., Chem. Commun.*, (1988) 834.
- [6] S.M. Stuczynski, Y.-U. Kwon and M.L. Steigerwald, *J. Organomet. Chem.*, **449** (1993) 167.
- [7] W. Inhof and G. Huttner, *J. Organomet. Chem.*, **448** (1993) 247.
- [8] P. Baistrocchi, D. Cauzzi, M. Lanfranchi, G. Predieri, A. Tiripicchio and M. Tiripicchio Camellini, *Inorg. Chim. Acta*, **235** (1995) 173.
- [9] D. Cauzzi, C. Graiff, M. Lanfranchi, G. Predieri and A. Tiripicchio, *J. Chem. Soc., Dalton Trans.*, (1995) 2321.
- [10] T. Chivers, D.D. Dosssee and R.W. Hiltz, *Inorg. Chem.*, **32** (1993) 3244.
- [11] N. Walker and D. Stuart, *Acta Crystallogr., Sect. A*, **39** (1983) 158; F. Uguzzoli, *Comput. Chem.*, **11** (1987) 109.
- [12] G.M. Sheldrick, *SHELXS-86*, program for the solution of crystal structures, Universität Göttingen, Germany, 1986.
- [13] G.M. Sheldrick, *SHELX-76*, program for crystal structure determination, University of Cambridge, UK, 1976.
- [14] *International Tables for X-Ray Crystallography*, Vol. IV, Kynoch, Birmingham, UK, 1974, pp. 99–102, 149.
- [15] A. Casoli, A. Mangia, G. Predieri, E. Sappa and M. Volante, *Chem. Rev.*, **89** (1989) 407.
- [16] J.A. Ramsden, C.M. Garner and J.A. Gladysz, *Organometallics*, **10** (1991) 1631.
- [17] M. Careri, A. Mangia, P. Manini, G. Predieri, V. Ravertino, G. Tsoupras and E. Sappa, *J. Chromatogr.*, **647** (1993) 79; M. Careri, A. Mangia, P. Manini, G. Predieri and E. Sappa, *J. Organomet. Chem.*, **476** (1994) 127.
- [18] M. Careri, G. Mori, G. Predieri, N. Souza de Rezende and E. Sappa, *J. Chromatogr.*, **634** (1993) 143.
- [19] C.F. Campana, F.Y.-K. Lo and L.F. Dahl, *Inorg. Chem.*, **18** (1979) 3060.
- [20] L.F. Dahl and P.W. Sutton, *Inorg. Chem.*, **2** (1963) 1067.
- [21] B.F.G. Johnson, T.M. Layer, J. Lewis, A. Martin and P.R. Raithby, *J. Organomet. Chem.*, **429** (1992) C41.